ECS Transactions, 7 (1) 1909-1918 (2007)
10.1149/1.2729303, ©The Electrochemical Society

Parameter Effects on Transport Phenomena in Conjunction with Internal Reforming Reactions in Intermediate Temperature SOFCs

Jinliang Yuan[a,*], Wei Guo Wang[b]

[a]Department of Energy Sciences, Faculty of Engineering
Lund University, Box 118, 22100 Lund, Sweden
[b]Ningbo Institute of Materials Technology and Engineering (NIMTE)
Chinese Academy of Sciences (CAS),
315040 Ningbo, P.R. China

Various transport phenomena in conjunction with chemical reactions are strongly affected by solid oxide fuel cells (SOFCs) configurations and properties of involved porous anode. The considered composite duct is relevant for an intermediate temperature (600-800°C) SOFC and consists of a porous anode layer for the internal reforming reactions of methane, the fuel gas flow duct, and a solid plate. In this paper, a three-dimensional calculation method is developed to simulate and analyze internal reforming reactions, to reveal the importance of design and operating parameters in three characteristic ratios. The SOFC conditions such as mass balances associated with the internal reforming reactions and gas permeation to/from the porous anode are applied in the analysis. The results show that the characteristic ratios have significant effects on the transport phenomena and overall reforming reaction performance.

Introduction

During recent years, the trend is to reduce the operating temperature of solid oxide fuel cells (SOFCs) to a moderate range (from 1000°C to 800°C) by employing a thick porous layer (1.5-2 mm) as the supporting structure (1-4). The size of the porous anode for this new design is bigger than that of the flow duct in terms of thickness and cross-sectional area. The transport rate of fuel gases to the active surface for electrochemical size, permeability, and volume percent porosity), pressure gradient between the fuel flow duct and the porous anode, gas composition and inlet conditions, etc. (5-7).

For the case of pure hydrogen being employed as the fuel, it is true that part of H_2 is consumed while water vapor (H_2O) is generated during the electrochemical reaction. This is simulated as a mass suction and injection V_m (or $Re_m=V_mD_h/\nu$), respectively, at the active wall on the anode side (6, 7). If hydrocarbon fuels are used as the fuels, it is a fact that the heat required to keep internal steam reforming can be provided by the electrochemical reactions in SOFCs. There are several advantages to have internal steam reforming of employed hydrocarbon fuels, for instances, the energy conversion efficiency will be much higher, and this benefit does not appear if the pure hydrogen is considered as the fuel. Moreover, close coupling of the internal reforming and the electrochemical reactions at the anode gives good heat transfer. Furthermore, hydrogen and CO are utilized by the cell as soon as they are produced by the reforming reaction, and the steam produced by the electrochemical reaction can be used in the reforming reaction as well

Downloaded 23 Oct 2009 to 60.190.58.162. Redistribution subject to ECS license or copyright; see http://www.ecsdl.org/terms_use.jsp

(8). However, most of the internal reforming reaction takes place in the porous anode next to the fuel gas flow duct due to the high methane conversion rate, and very little methane reaches the active surface between the electrolyte and the porous anode. The endothermic internal reforming reaction and the exothermic electrochemical reactions are separated, and consequently may lead to certain temperature gradients in the porous layer.

In this study, various fundamental phenomena and parameter effects are investigated, with the purpose to provide improved understanding and to supply guidance for the practical implementation of such a design. Based on three characteristic ratios proposed in this paper, studies have been conducted for various engineering parameters which are relevant for the SOFC design, and effects on the transport processes in conjunction with chemical reactions are presented and discussed in terms of various parameters, such as the species distributions, chemical reaction rates and overall methane conversions, etc.

Problem Statement and Formulations

With heat generation by the electrochemical reactions in the SOFC stack, internal reforming of hydrocarbon fuels takes place at the anode of the cells with steam. The section of the anode, where reforming occurs, is adjacent to the place where the electrochemical reaction appears, the heat from the fuel cell electrochemical reactions is supplied for the reforming reaction by internal heat transfer with minimal losses.

Methane and carbon monoxide can be reformed into H_2 by the following reactions:

$$CH_4 + H_2O \rightarrow CO + 3H_2 \qquad \Delta H_{1000\ K} = 226\ kJ/mol \qquad [1]$$
$$CO + H_2O \rightarrow CO_2 + H_2 \qquad \Delta H_{1000\ K} = -35\ kJ/mol \qquad [2]$$

Equation [2] is usually referred to as water-gas shift reaction. It should be mentioned that the above process in Eq. [1] is endothermic and the overall balance of the reaction requires net heat input by the electrochemical reaction.

The electrochemical reactions to generate electricity are the oxidation of H_2 and CO:

$$H_2 + O^{2-} \rightarrow H_2O + 2e^- \qquad [3]$$
$$CO + O^{2-} \rightarrow CO_2 + 2e^- \qquad [4]$$

The above reactions produce a significant amount of the water at the anode side during operation.

A three-dimensional computational fluid dynamics (CFD) code is employed for an anode duct of a typical reduced temperature SOFC design, see Fig. 1a. A schematic structure of the anode duct is shown in Fig. 1b. The U, V, and W are the velocity components in the x, y, z directions, respectively. In this study, the porous anode layer is assumed to be homogeneous and characterized by effective parameters and the fuel in the porous layer is in thermal equilibrium with the solid matrix. The electrochemical reaction appears at the interface between the electrolyte and the porous layer (bottom surface in Fig. 1b), while the internal reforming reactions are within the porous layer. A constant flow rate $U=U_{in}$ with a mass fraction of the mixed fuel is specified at the inlet of the gas

Downloaded 23 Oct 2009 to 60.190.58.162. Redistribution subject to ECS license or copyright; see http://www.ecsdl.org/terms_use.jsp

flow duct, while $U=0$ is specified at the inlet for the inter-connector and porous anode layer. Only the right half of the duct is considered by imposing symmetry conditions on the mid-plane.

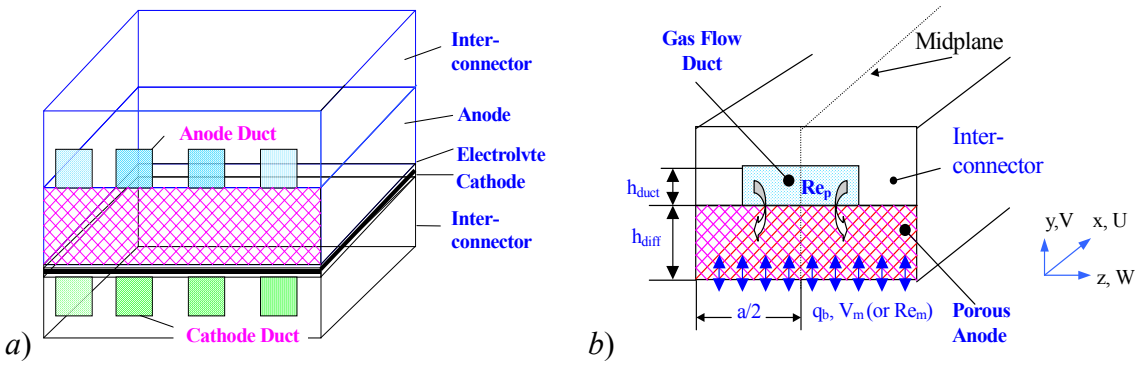

Figure 1. a) Structure of a unit cell; b) schematic drawing of a composite anode duct.

The governing equations to be solved are the continuity, momentum, energy and species equations. The mass continuity equation is written as

$$\nabla \bullet (\rho_{eff} \mathbf{v}) = S_m \qquad [5]$$

The source term S_m in the above equation accounts for the mass balance due to the electrochemical reactions.

$$S_m = (J_{H_2} + J_{CO} + J_{H_2O}) \frac{A_{active}}{V} = (-\frac{i_{H_2}}{2F} M_{H_2} - \frac{i_{CO}}{2F} M_{CO} + \frac{i_{H_2} + i_{CO}}{2F} M_{H_2O}) \frac{A_{active}}{V} \qquad [6]$$

where, V refers to control volume, (i_{H2}+ i_{CO}) is the total current density i passing through the cell. The momentum equation reads

$$\nabla \bullet (\rho_{eff} \mathbf{VV}) = -\nabla P + \nabla \bullet (\mu_{eff} \nabla \mathbf{V}) + S_{di} \qquad [7]$$

The inclusion of the source term S_{di} allows Eq. [7] to be valid for both the porous layer and the flow duct:

$$S_{di} = -(\mu_{eff} \mathbf{V} / \beta) - \rho_{eff} B V_i |\mathbf{V}| \qquad [8]$$

The first term on the right hand side of the above equation accounts for the linear relationship between the pressure gradient and flow rate according to Darcy's law. The second term is the Forchheimer term which takes into account the inertial force effects, i.e., the non-linear relationship between pressure drop and flow rate (7). In Eq. [8], β is the porous layer permeability, and $\boldsymbol{V}$ represents the volume-averaged velocity vector of the species mixture.

The energy equation can be expressed as:

$$\rho_{eff} c_{p,eff} \nabla \bullet (\mathbf{v}T) = \nabla \bullet (k_{eff} \nabla T - \sum_{i=1}^{n} \dot{\mathbf{m}}_i h_i) + S_T \qquad [9]$$

Downloaded 23 Oct 2009 to 60.190.58.162. Redistribution subject to ECS license or copyright; see http://www.ecsdl.org/terms_use.jsp

Equation [9] balances the convected energy, the heat conduction through the solid and the gas mixture, the energy due to fuel gas species diffusion, and a source term S_T. It should be mentioned that the gas species diffusion related thermal energy is accounted for in both the gas flow duct and the porous anode. In Eq. [9] h_i is the partial enthalpy of the ith species where S_T is the heat source associated with the steam reforming and water-gas shift reactions,

$$S_T = R_{ir} h_{ir} \qquad [10]$$

R_{ir} is the reaction mass flux by the internal reforming, and h_{ir} is the reaction enthalpy.

The species conservation equations are formulated in a general form,

$$\nabla \bullet (\rho_{eff} \mathbf{V} Y_i) = \nabla \dot{\mathbf{m}}_i + S_{s,i} \qquad [11]$$

where Y_i is the mass fraction of the ith fuel gas species, $\dot{\mathbf{m}}_i$ represents the mass diffusive flux of species in units of kg/(m^2 s), and $S_{s,i}$ the production/consumption rate of the ith fuel species. The above equation is solved for H_2, CH_4, CO and H_2O, respectively, i.e., for n-1 species where n is the total number of species involved in the fuel gas mixture. The last species (CO_2) can be solved because the sum of the mass fractions equals one.

Mass diffusion is a process leading to equalization of substance concentration or establishing an equilibrium gas distribution that results from random migration of the species. Molecular diffusion occurs as a result of thermal motion of the molecules, and proceeds at a maximum rate in gases, a lower rate in liquids, and at a still lower rate in solids (10). In the general case, the molecular diffusion flux of the species i is proportional to the concentration gradient and diffusion coefficient. One of the significant challenges in fuel cell modeling is in determining the rate at which the species diffuse and gases convect in the gas flow ducts and porous electrodes. This requires knowledge of multi-component diffusion in the fuel gas flow ducts, particularly in the porous layers. In the literature, there are several basic approaches for determining the molar diffusion flux $\dot{\mathbf{n}}_i$ and converting to mass diffusion flux $\dot{\mathbf{m}}_i$ via the species molar mass, i.e., $\dot{\mathbf{n}}_i = \dot{\mathbf{m}}_i / M_i$. Fick's law, represented by $\dot{\mathbf{n}}_i = -\rho D_{i,j} \nabla X_i$ based on binary diffusion coefficient $D_{i,j}$ and molar fraction X_i, is the simplest diffusion model and is typically used in binary or dilute system (10). A multi-component extension of Fick's law is sometimes used in the literature as well, e.g., in (11),

$$\dot{\mathbf{n}}_i = -\rho D_{i,j} \nabla X_i + X_i \sum_{i=1}^{n} \dot{\mathbf{n}}_j \qquad [12]$$

while the Stefan-Maxwell model is more commonly used in multi-component system, as in this study. The diffusion coefficients of species i in the fuel gas flow duct is calculated by the expression based on the binary coefficients (10)

$$D_{A,gm} = \frac{1 - X_A}{X_B / D_{AB} + X_C / D_{AC} + \ldots} \qquad [13]$$

where $D_{A,gm}$ is the diffusion coefficient of the component A in the mixture with B, C, …, X_A, X_B, X_C are the molar fraction of the appropriate species, and D_{AB} and D_{AC} are the

Downloaded 23 Oct 2009 to 60.190.58.162. Redistribution subject to ECS license or copyright; see http://www.ecsdl.org/terms_use.jsp

diffusion coefficients in the *AB* and *AC* binary system, respectively. It is clear that for an *n* component system, *n*(*n*-1)/2 binary diffusivities are required.

For the porous layer, molecular diffusion is predominant in the case with large pores, whose size is much bigger than the free-path of the diffusion gas molecules. In this case, the diffusion can be described as above presented for the fuel gas flow duct. Knudsen diffusion occurs in the porous layer with small pores or under low pressure when the mean free-path of molecules is smaller than the pore size, and the molecules collide with the walls more often than between themselves. In order to calculate the Knudsen diffusion flux, the coefficient $D_{i,k}$ is calculated based on the free molecule flow theory (10):

$$D_{i,k} = \frac{2}{3} r_e v_i = \frac{2}{3} r_e \left(\frac{8\Re T}{\pi M_i}\right) \qquad [14]$$

in which r_e is the effective radius and v_i the average molecular speed of the *i*th fuel species. To account for the reduction in the cross-sectional area and the increased diffusion length due to the tortuous paths of real pores in the porous anode, the effective diffusion coefficient can be evaluated (9, 10):

$$D_{i,eff} = \frac{\varepsilon}{\tau}\left(\frac{D_{i,gm} \times D_{i,k}}{D_{i,gm} + D_{i,k}}\right) \qquad [15]$$

where ε is the porous anode porosity, τ tortuosity. The most common anode is based on nickel/zirconia cermet which can provide sufficient activity for the steam reforming and water-gas shift reactions without the need for any additional catalyst (9). There exist various reaction kinetics and rate/equilibrium constants reported in the literature for both the steam reforming and water-gas shift reactions. However, based on extensive reviews in (8, 9), it can be found that the rate data presented in the literature varies greatly due to the use of different material structures and different amount of catalyst. In this study, the following reaction rates are employed to express the kinetic rates of absorption or production of the fuel gas species, based on partial pressure, temperature and species compositions:

$$R_r = k_r^+ p_{CH_4} p_{H_2O} - k_r^- p_{CO} (p_{H_2})^3 \qquad [16]$$

$$R_s = k_s^+ p_{CO} p_{H_2O} - k_s^- p_{CO_2} p_{H_2} \qquad [17]$$

in which, k^+ and k^- are velocity constants of the forward and backward reactions, *p* partial pressure. Then, $S_{s,i}$ in Eq. [11] reads:

$$\begin{aligned} S_{s,H_2} &= (3R_r + R_s) M_{H_2}; S_{s,CH_4} = -R_r M_{CH_4}; \\ S_{s,H_2O} &= (-R_r - R_s) M_{H_2O}; S_{s,CO} = (R_r - R_s) M_{CO} \end{aligned} \qquad [18]$$

Numerical Solution Procedure

A three-dimensional CFD code was used to solve the governing equations together with the boundary conditions and interfacial conditions. The code is a general purpose one and based on the finite-volume technique with boundary fitted coordinates for solving the differential equations. The Cartesian coordinate system in the physical space is replaced by a general non-orthogonal coordinate system. The momentum equations are

Downloaded 23 Oct 2009 to 60.190.58.162. Redistribution subject to ECS license or copyright; see http://www.ecsdl.org/terms_use.jsp

solved for the velocity components on a non-staggered grid arrangement. The Rhie-Chow interpolation method is used to compute the velocity components at the control volume faces. Algorithms based on the TDMA and a modified SIP are employed for solving the algebraic equations. In this study, the convective terms are treated by the QUICK scheme, while the diffusive terms are treated by the central difference scheme. The SIMPLEC algorithm handles the linkage between velocities and pressure.

Parameters of ITSOFCs and the porous anode configuration, appearing in the common literature, are applied as a base case in this study. Duct geometries are employed as follows: length of the duct L=20mm; width of the porous layer a=2mm, and its thickness h_p=2mm; while the width of the flow duct is b=1mm, and its height h_d=1mm. Fuel gas inlet conditions are: temperature T_{in}=800^oC, partially (30%) prereformed methane/steam mixture with: Re_{in}=50, molar concentration X_{H2}:X_{CH4}:X_{CO}:X_{H2O}:X_{CO2}=0.284:0.171:0.028: 0.473:0.044; In the porous layer, typical values are employed for porosity ε=0.5, tortuosity τ=3, and permeability β=2×10$^{-10}m^2$; The binary diffusion coefficients of the fuel species are shown in Table 1. In this study, a constant total current density i = 0.6 A/cm^2 is prescribed, however this limitation will be released in future investigations when the electrolyte is included. It should be noted that all the results presented hereafter are for the base case condition unless otherwise stated, such as sensitive parameter studies.

Table 1. Binary diffusivity of the ith fuel gas species at T=1123.15 K, p=1.013 bar (4).

i/j	***$D_{i,j}$ (m^2/s)***	***i/j***	***$D_{i,j}$ (m^2/s)***
CH_4/CO	3.47e-05	CO/H_2	11.92e-05
CH_4/H_2O	4.30e-05	CO/CO_2	2.59e-05
CH_4/H_2	11.04e-05	H_2O/H_2	14.10e-05
CH_4/CO_2	2.88e-05	H_2O/CO_2	3.38e-05
CO/ H_2O	4.15e-05	H_2/CO_2	10.23e-05

Results and Discussion

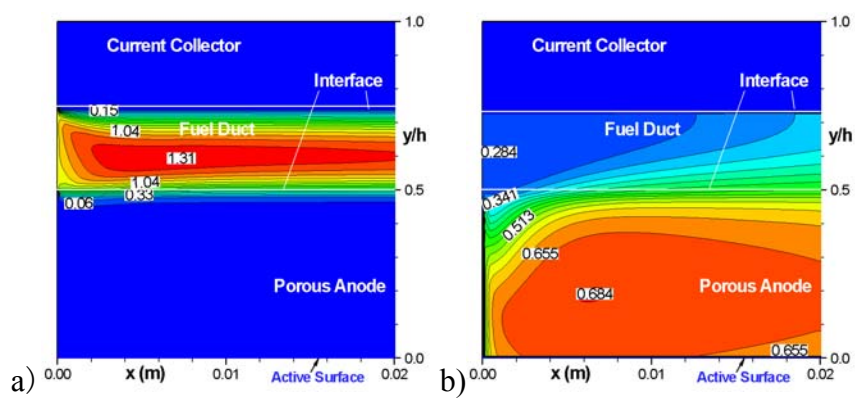

Figure 2. a) Dimensionless axial velocity contours (U/U_{in}); b) H_2 mole fraction along the main flow stream of an SOFC anode duct at the base case condition.

Axial velocity contours (U/U_{in}) are presented for an intermediate temperature SOFC anode duct in Fig. 2a. As mentioned above, gas flow and heat transfer in the composite ducts are affected by the internal reforming reactions in the porous layer and the electrochemical reactions close to the active surface. It is found that the position of the

Downloaded 23 Oct 2009 to 60.190.58.162. Redistribution subject to ECS license or copyright; see http://www.ecsdl.org/terms_use.jsp

maximum contour values shifts away from the central plane (y/h = 0.625 in Fig. 2*a*), and the axial velocity magnitude of the fuel mixture decreases rapidly in the porous layer. On the other hand, the active surface is sufficiently supplied with H_2 resulting from both the steam reforming and water-gas shift reactions. Moreover, the H_2 mole concentration is affected by the mass consumption from the electrochemical reactions, as shown in Fig. 2*b*.

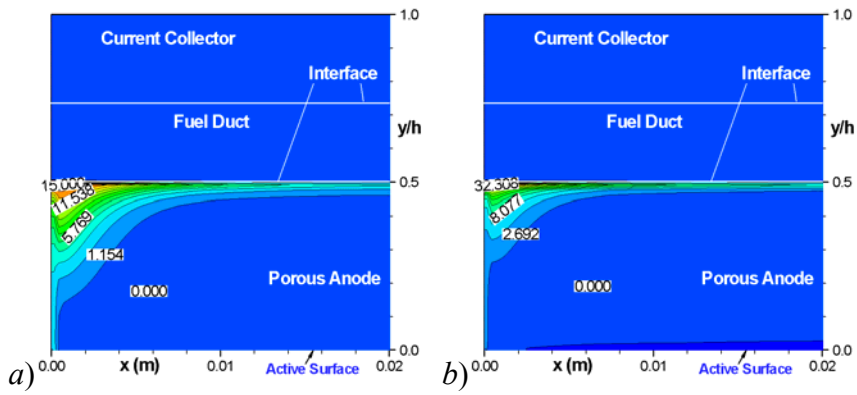

Figure 3. Distribution of: *a*) steam reforming reaction; *b*) water gas-shift reaction rate along main flow direction of an SOFC anode duct.

The steam reforming reaction and the shift reaction rates are shown in Figs. 3*a* and *b*, respectively. It is found that both reactions are strong at the interface and the entrance regions within the porous layer close to the fuel flow duct (with big reaction rate value). No reactions can be observed in the rest of the porous anode, particularly after a certain distance downstream the inlet. The distance for this specific case is about half the duct length.

Three characteristic ratios, having significant effects on various transport processes and chemical reactions as discussed later in this paper, are defined in this section. These are the hydraulic diameter ratio D_{hr} (ratio of the porous layer diameter to the flow duct diameter), the permeation length ratio PL_r (ratio of the fuel flow duct width to the porous catalyst layer width), and the permeation rate ratio PR_r (ratio of the entrance pressure gradient to permeation resistance).

$$D_{hr}=D_{hp}/D_{hd} \qquad [19]$$

$$PL_r=a/b \qquad [20]$$

$$PRr=(\rho U_{in}^2/2h_p)/(\mu U_{in}/\beta_i)=(\rho\beta_i U_{in})/(2\mu h_p) \qquad [21]$$

D_{hp} in Eq. [19] is the hydraulic diameter of the porous anode, D_{hd} the hydraulic diameter of the fuel flow duct; a in Eq. [20] is the width of gas flow duct, b the width of the porous anode; h_p in Eq. [21] is the thickness of the porous anode. It is clear that both diameter ratio D_{hr} and permeation length ratio PL_r are related to the fuel flow duct and porous anode configurations, to account for the characteristics of the permeation area and length, respectively. The permeation rate ratio PR_r considers the characteristics of the porous material (such as the permeability β_i) and duct operation parameter (such as the inlet velocity U_{in}).

Downloaded 23 Oct 2009 to 60.190.58.162. Redistribution subject to ECS license or copyright; see http://www.ecsdl.org/terms_use.jsp

Effects of the Diameter Ratio (D_{hr} =1.67, 2.33 vs. 2.0)

To investigate effects of the diameter ratio on the transport phenomena and reforming reactions, the height of fuel flow duct h_d was varied. Figure 4 shows velocity contours for the cases of D_{hr} =2.33 (h_d =0.75 mm) and D_{hr} =1.67 (h_d =1.6 mm) (the base case D_{hr} =2, h_d =1.0 mm). It should be noted that the height of the upper solid plate was changed accordingly to keep the total height of the upper solid plate and the fuel flow duct constant.

As shown in Fig. 4, the velocity contours for big or small D_{hr} have a similar trend as that of the base case, i.e., there is no symmetry of the axial velocity and the position of the maximum values shifts away from the physically central plane. This effect is more significant for the big D_{hr} case (shown in Fig. 4*a*), if compared to the one with small D_{hr} (shown in Fig. 4*b*). More critically, more fuel gas is permeated to and kept in the porous reaction region, as shown in Fig. 4*a* with smaller velocity contours than those in Fig. 4*b*. This may be due to the fact that the fuel gas flow duct in Fig. 4*a* is small if compared to the porous anode layer.

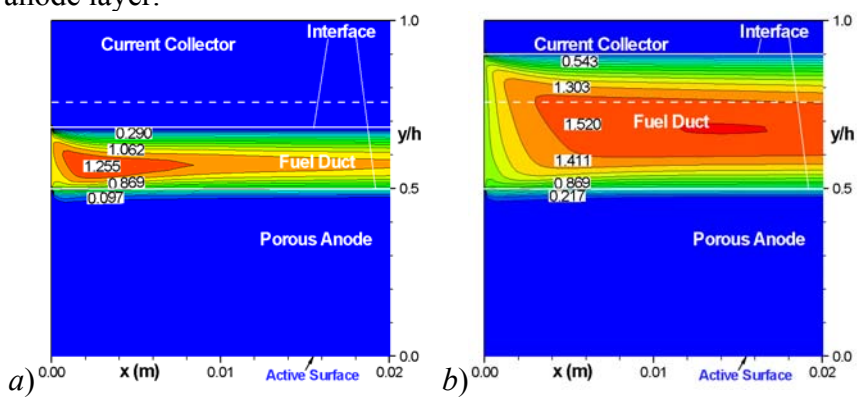

Figure 4. Velocity contours for the cases of: *a*) D_{hr} =2.33; *b*) D_{hr} =1.67.

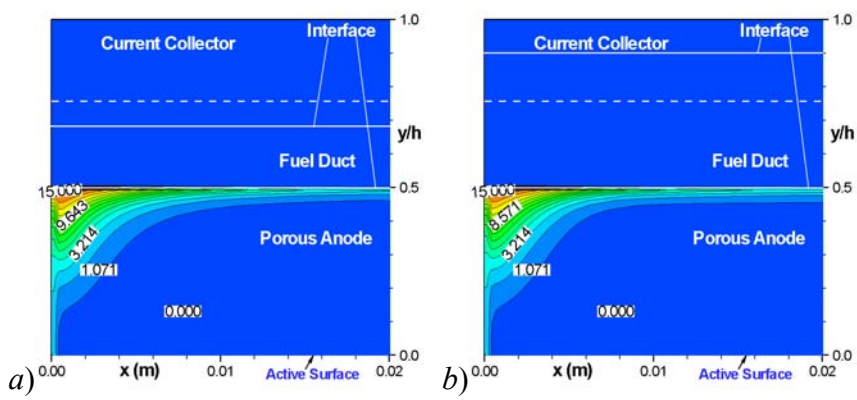

Figure 5. Distribution of reforming reaction for the cases of: *a*) D_{hr} =2.33; *b*) D_{hr} =1.67.

On the other hand, almost the same steam reforming reaction rates are obtained for both cases, as shown in Fig. 5. This finding is also true for the water gas-shift reaction, in terms of maximum reaction rates. However, a big methane conversion can be found for the case of the big D_{hr}. This means that the diameter ratio has more significant effects on the fuel gas flow in both fuel flow duct and the porous anode than those on the chemical reactions. It is believed that the high methane conversion obtained in the case of big D_{hr} is mainly due to the fact that the fuel gas flow rate is small when the fuel flow duct is small or the diameter ratio D_{hr} is big.

Downloaded 23 Oct 2009 to 60.190.58.162. Redistribution subject to ECS license or copyright; see http://www.ecsdl.org/terms_use.jsp

Effects of Permeation Length (PL_r =0.375, 0.8 vs. 0.5)

Effects of the permeation length ratio have been investigated as well by varying the width of the fuel flow duct *b*, while other ratios were kept constant. Permeation length ratios PL_r =0.375 (*b*=0.375 *mm*) and PL_r =0.8 (*b*=0.8 *mm*) were employed, and the predicted performance is compared with that of the base case (PL_r =0.5, *b*=0.5 *mm*). From Fig. 6, it is found that the cross-section velocity profiles are similar to each other for different permeation length ratios. Moreover, the steam reforming reaction rate for the case with small permeation length ratio (Fig. 6*a*) is almost in the same order as that achieved in the case with big permeation length ratio (Fig. 6*b*). However, the methane conversion efficiency is high for the latter case, due to its longer permeation length, i.e., longer reaction length. This reveals that the permeation length ratio puts more significant effects on the fuel gas permeation between the fuel flow duct and the porous anode, and then the methane conversion.

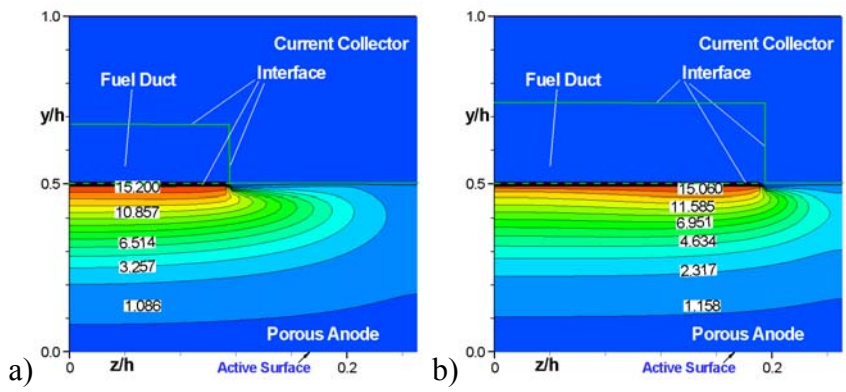

Figure 6. Distribution of steam reforming reaction at the inlet cross section for the cases of: *a*) PL_r =0.375; *b*) PL_r =0.8.

Effects of the Permeation Rate Ratio (Permeability)

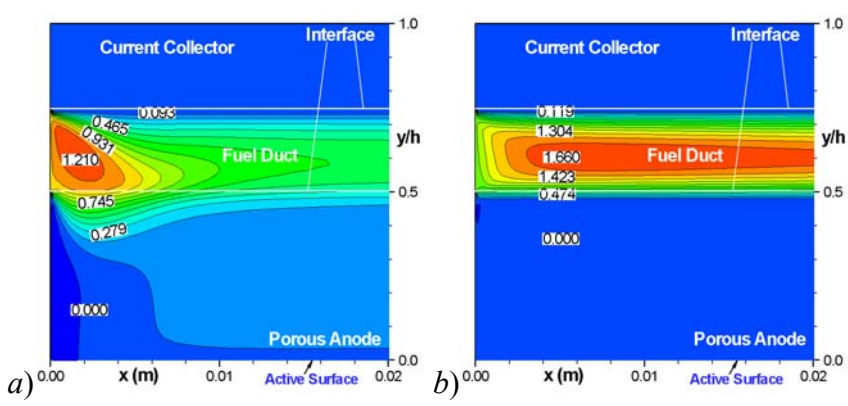

Figure 7. Effects of the permeation rate ratio (permeability) on the dimensionless axial velocity contours at: *a*) β=2.0×10^{-9} m^2; *b*) β = 2.0×10^{-11} m^2.

Figure 7 shows the impact of the porous anode permeability on the fuel gas flow. As for a big permeability in Fig. 7*a*, more fuel gas is permeated from the flow duct, and as a result the gas convection can be clearly found with certain velocities in the porous anode. Consequently, more significant impacts on the change of the axial velocity distribution are expected for both the flow duct and the porous anode, when the permeability is higher.

Downloaded 23 Oct 2009 to 60.190.58.162. Redistribution subject to ECS license or copyright; see http://www.ecsdl.org/terms_use.jsp

It is noted from Fig. 7*b* that, by decreasing the permeability, fuel gas permeation to the porous anode is small, i.e., the axial velocity is zero for the most regions of the porous anode. Furthermore, the velocity in the fuel flow duct is similar to the parabolic one associated with the pure duct flow. This is so because the permeability is a term used for the conductivity of the porous medium with respect to permeation by a fluid. It is known that a small permeability of a porous layer allows less gas to pass at the same pressure gradient.

Conclusions

A fully three-dimensional calculation method has been further developed to simulate and analyze gas flow and heat transfer processes in a thick anode duct of SOFCs. The model offers the possibilities of determining temperature and fuel gas species distribution profiles by taking into account of the internal reforming reactions and the electrochemical reactions. Results from this study show that the internal reforming reactions are confined in a thin porous anode area close to fuel flow duct. Transport processes of the fuel gas species and temperature distribution are affected by the reactions.

References

1. A. V. Virkar, J. Chen, C. W. Tanner, and J. W. Kim, *Solid State Ionics*, **131**, 189 (2000).
2. H. Yakabe, M. Hishinuma, M. Uratani, Y. Matsuzaki, and I. Yasuda, I., *J. Power Sources*, **86**, 423 (2000).
3. W. Lehnert, J. Meusinger, and F. Thom, *J. Power Sources*, **87**, 57 (2000).
4. T. Ackmann, L. G. J. Haart, W. Lehnert, and F. Thom, p. 431, *Proc. 4th European Solid Oxide Fuel Cell Forum,* Lucerne, Switzerland (2000).
5. J. Yuan, M. Rokni, and B. Sundén, *Int. J. Heat Mass Transfer*, **46**, 809 (2003).
6. J. Yuan, M. Rokni, M. and Sundén, B., *Fuel Cell Science, Engineering and Technology*, R. K. Shah and S. G. Kandlikar (eds.), p. 209, FUELCELL2003-1721, ASME (2003).
7. J. Yuan, M. Faghri, and B. Sundén, *Transport Phenomena in Fuel Cells*, B. Sundén & M. Faghri (eds.), MIT Press (2005).
8. A. Aguiar, C. S. Adjiman, and N. P. Brandon, *J. Power Sources*, **138**, 120 (2004).
9. B. A. Haberman and J. B. Young, *Int. J. Heat Mass Transfer*, **47**, 3617 (2004).
10. I. L. Mostinsky, *International Encyclopedia of Heat & Mass Transfer*, G. F. Hewitt, G. L. Shires, and Y. V. Polezhaev, (eds.), CRC Press, Florida, USA (1996).
11. J. R. Ferguson, J. M. Fiard, and R. Herbin, *J. Power Sources*, **58**, 109 (1996).
12. B. Alazmi and K. Vafai, *Int. J. Heat and Mass Transfer*, **44**, 1735 (2001).
13. C. Borgnakke and R. E. Sonntag, *Thermodynamic and Transport Properties*, John Wiley & Sons (1997).

Downloaded 23 Oct 2009 to 60.190.58.162. Redistribution subject to ECS license or copyright; see http://www.ecsdl.org/terms_use.jsp